Available online at www.sciencedirect.com
SCIENCE DIRECT®
Journal of Sound and Vibration 291 (2006) 706–722
JOURNAL OF SOUND AND VIBRATION
www.elsevier.com/locate/jsvi

Active flutter suppression of a lifting surface using piezoelectric actuation and modern control theory

Jae-Hung Han[a,*], Junji Tani[b], Jinhao Qiu[b]

[a]*Department of Aerospace Engineering, Korea Advanced Institute of Science and Technology, 373-1 Guseong-Dong Yuseong-Gu, Daejeon 305-701, Republic of Korea*
[b]*Institute of Fluid Science, Tohoku University, 2-1-1 Katahira Aoba-ku, Sendai 980-8577, Japan*

Received 26 August 2003; received in revised form 17 August 2004; accepted 23 June 2005
Available online 3 October 2005

Abstract

This paper presents a numerical and experimental investigation on active flutter suppression of a swept-back cantilevered lifting surface using piezoelectric (PZT) actuation. A finite element method, a panel aerodynamic method, and the minimum state–space realization are involved in the development of the equation of motion in state–space, which is efficiently used for the analysis of the system and design of control laws with a modern control framework. PZT actuators, bonded symmetrically on the plate, are optimally grouped into two equivalent actuator sets using genetic algorithms to enhance controllability. H_2- and μ-synthesized control laws are designed and the flutter suppression performance is evaluated via wind tunnel testing. In the μ-synthesis design, a simple parametric uncertainty model is used to take into account the system changes with respect to airflow speed. Both controllers show comparable flutter suppression performance around the flutter point. However, the μ-synthesized controller shows improved behavior over a wide flow speed range.
© 2005 Elsevier Ltd. All rights reserved.

1. Introduction

There have been intensive efforts to understand aeroelastic behavior more accurately in order to avoid serious aeroelastic problems such as stability margin reduction and catastrophic structural

*Corresponding author. Tel.: +82 42 869 3723; fax: +82 42 869 3710.
E-mail address: jaehunghan@kaist.ac.kr (J.-H. Han).

0022-460X/$ - see front matter © 2005 Elsevier Ltd. All rights reserved.
doi:10.1016/j.jsv.2005.06.029

failure due to excessive vibration. Recent aircraft designs employ more lightweight materials and structures so that various aeroelastic problems may happen more frequently. In recent years, applications of active control to aeroelastic systems have been studied in order to favorably modify the behavior of aeroelastic systems [1].

Flutter suppression is one of the main objectives of the aeroelastic control. Control surfaces such as spoilers and flaps have been generally used to generate auxiliary aerodynamic lift and moment. The active flexible wing (AFW) program has demonstrated flutter suppression of a fighter-type scaled model in various maneuver modes by utilizing control surfaces and active control technology at NASA Langley research center [2–4]. The Benchmark Active Control Technology (BACT) model has been used as an active control test bed for evaluating new and innovative control methodologies [5,6]. Vipperman et al. [7,8] developed a wind tunnel model of a typical section airfoil with a trailing-edge flap and applied H_2- and μ-synthesized controls for active flutter suppression. They reported that μ-synthesized control provided significantly better disturbance rejection than H_2 controller, particularly when the aeroelastic pole migration is dominant. Block and Strganac [9] constructed a unique test apparatus for the experiments of plunge and pitch motion with prescribed stiffness characteristics. They investigated linear and nonlinear aeroelastic responses and controlled flutter phenomena using an optimal observer and a full-state feedback.

In addition to experimental research, many control strategies have been developed for active flutter suppression. Roy and Eversman [10] investigated the potential use of an adaptive feedforward controller based on the filtered-X least mean squares (LMS) algorithm for active flutter suppression of a flexible wing. Zeng and Singh [11] derived the control algorithms for pitch angle and plunge displacement trajectory control on the basis of the variable structure adaptive model reference control theory. Barker et al. [12] applied gain-scheduling techniques to track the system changes due to various flow conditions. Yang et al. [13] studied semi-active control of structural nonlinear flutter. In accordance with the theoretical analysis, a wind tunnel test model was developed with a micromotor-slide block system as the parameter control executive element. Gade and Inman [14] proposed an active decoupler pylon for the improvement of the stability robustness of an active wing/store flutter suppression system.

Recent development of smart or intelligent structures gives us another alternative for active flutter suppression [15]. Among several functional materials, piezoelectric (PZT) materials have drawn attention as possible actuation mechanisms for flutter prevention systems because of their simple structure and fast response time [16]. Lazarus et al. [17] successfully applied linear quadratic Gaussian (LQG) controls to suppress vibration and flutter of a plate-like lifting surface with surface-bonded PZT actuators. Application of PZT actuation to flutter control of a more realistic wing model was achieved under the piezoceramic aeroelastic response tailoring investigation (PARTI) program at NASA Langley research center [18]. Active flutter controls of wing boxes and panels have also been investigated using PZT strain actuators [19,20].

This paper investigates active flutter suppression of a swept-back cantilevered plate using PZT actuation. The present work is based on the study by Lazarus et al. [17]; the main improvements lie in the study of actuator placement and the application of modern robust control theory.

The aeroelastic model of the plate has been determined in the state–space representation form using a finite element method, a panel aerodynamic method, and a rational function approximation. The dynamic and actuation characteristics of generally shaped lifting surfaces with distributed PZT actuators can be easily analyzed using the finite element code developed by

Han and Lee [21]. The doublet-lattice method (DLM) panel aerodynamic code is used to obtain unsteady aerodynamics in this study [22]. There are many methods of rational function approximations for unsteady aerodynamic forces, but the minimum state–space realization by Karpel and Hoadley [23] is used to keep the number of states minimum. The obtained state–space aeroelastic equations enable us to efficiently analyze the system and design controllers with a modern control framework.

Actuator placement problems are also studied in this paper. Only a few studies have been performed on the actuator location and selection for flutter suppression [24,25]. In this study, PZT actuators, bonded symmetrically on the plate, are optimally grouped into two equivalent actuator sets using genetic algorithms to enhance controllability.

H_2- and μ-synthesized control laws are designed and the effectiveness of the flutter suppression system is evaluated via wind tunnel testing. The preparation of the specimen and the experimental procedures are described. In the μ-synthesis design, a simple parametric uncertainty model is used to take into account the system changes with respect to airflow speed. Finally, the experimental results are provided in time and frequency domains, and the performances of the two control methods are compared.

2. System description

2.1. Test article

The test article is a swept-back cantilevered plate with symmetrically surface-bonded PZT actuators as shown in Fig. 1. The article has a span of 40 cm and a chord of 20 cm, respectively,

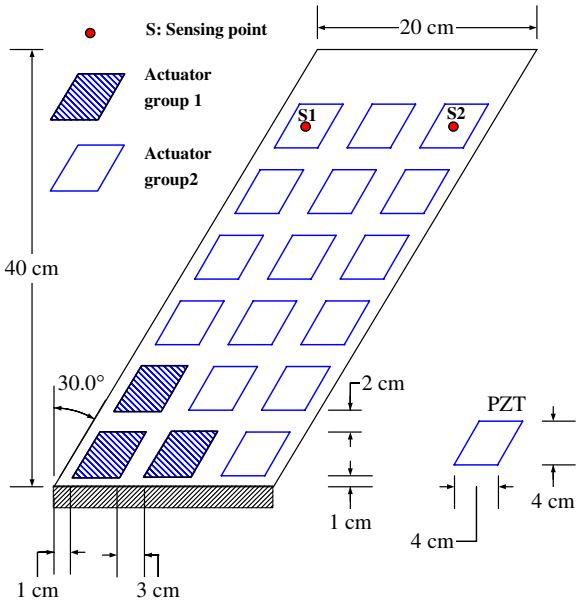

Fig. 1. Configuration of the test model.

Table 1
Material properties of the base plate and PZT

Property	Base plate (A1080)	PZT (C-91)
Young's modulus, E (GPa)	68.6	59
Shear modulus, G (GPa)	25.5	21.5
Density, ρ (kg/m^3)	2700	7750
Piezo constant, d (m/V)	—	-330×10^{-12}

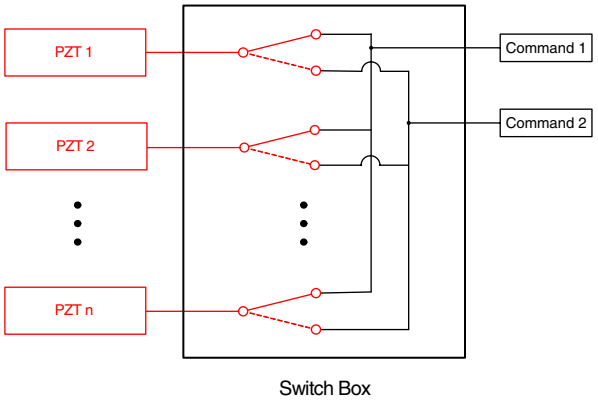

Fig. 2. Switch box to connect each PZT to the given command.

and the swept-back angle is 30°. The base plate is made of A1080 aluminum and the thickness of the plate is 0.45 mm. The swept-back configuration provides bending–torsion coupling of the structure so that the flutter speed can be lowered enough within wind tunnel operating speeds. Eighteen PZT patches (Fuji Ceramics® C-91, thickness: 0.2 mm) are bonded on each surface of the base plate. The material properties of the base plate and PZT actuator are presented in Table 1. The base plate is used as common electrical ground and very thin electric wires are connected to each actuator patch. Each electric line is connected to a switch box in such a way that multiple actuators can be commanded by a single control signal as shown in Fig. 2.

2.2. Wind tunnel

The wind tunnel testing was performed in the low-turbulence wind tunnel at the Institute of Fluid Science, Tohoku University in Japan. The wind tunnel is a closed-circuit tunnel with an effective velocity range of 5–70 m/s. Both open and closed test-sections are available, and in this paper, the open section was chosen to provoke aerodynamic disturbance. Fig. 3 shows the experimental setup in the wind tunnel. The nozzle is octagonal in shape and the distance between two facing sides is 1100 mm so that the effective testing section is approximately circular with a diameter of 1000 mm.

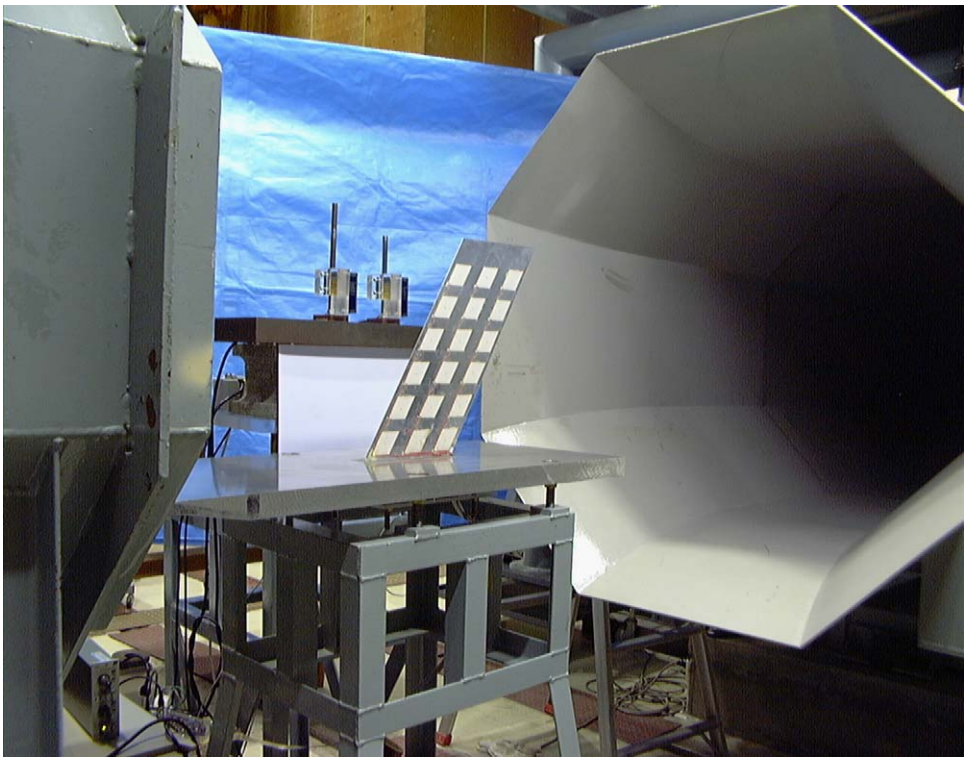

Fig. 3. Photograph of the experimental setup.

2.3. Sensor and controllers

Two long-range laser displacement sensors (Keyence® LB-300) are used to measure the displacements of the plate. The effective range of the sensors is 200–400 mm and they are located 300 mm from the plate. The influence of the sensors on the airflow is negligible. Note that actual applications of active flutter control need space-realizable sensors such as strain gages or accelerometers.

All control designs are implemented on a DSP board (dSPACE® DS1102). The DSP board has a Texas Instrument® TMS320C30 DSP chip as the main processor, and is equipped with 4 analog-to-digital and 4 digital-to-analog conversion channels. The sampling frequency used is 2 kHz, which is high enough compared with the dominant frequency band of the test article. An FFT analyzer (Onosokki® CF-3400) was used to record and process sensor and control signals.

3. Numerical model

Controller design for flutter suppression needs an accurate numerical model. Even though some previous studies have utilized system identification techniques to obtain numerical models, it is difficult, in many cases, to get sufficiently accurate numerical models that can be the function of

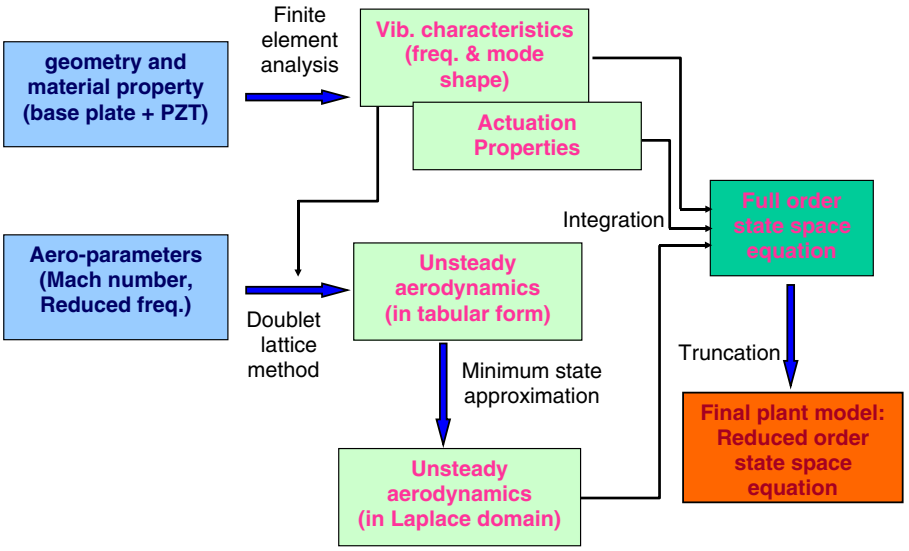

Fig. 4. Flowchart to obtain numerical model of the system.

velocity, air density, Mach number, and so on. Fortunately, numerical procedures for an aeroelastic model of a lifting surface in subsonic flow are well established. In this paper, the aeroelastic model of the test article is determined in the state–space representation form using a finite element method, a panel aerodynamic method, and a rational function approximation. Fig. 4 shows the flow chart for the numerical modeling procedure used in this paper. With given geometry and material properties of the test article, the vibration and actuation characteristics are obtained using the finite element method. The calculated modal characteristics are used to obtain unsteady aerodynamics in tabular form for various airflow parameters. The minimum state-approximation procedure, which was developed by Karpel and Hoadley [23], is applied to convert the unsteady aerodynamics into Laplace domain aerodynamics. A full order state–space system model is constructed by integrating vibration, actuation and sensing characteristics of the test article, and the resulting aerodynamics. Truncating less important states in Hankel singular value (HSV) sense yields a final plant model, which can be readily used for controller design. This section outlined these numerical procedures.

3.1. Structural model

By applying the finite element procedure by Han and Lee [21], the equation of motion for the swept-back cantilevered plate with distributed actuators can be obtained as follows:

$$[M]\{\ddot{u}\} + [K]\{u\} = \sum_{L=1}^{M} \{F_L\} V_L(t), \tag{1}$$

where $[M]$, $[K]$, and $\{u\}$ are the global mass and stiffness matrices, and the nodal displacement vector, respectively, $\{F_L\}$ and $V_L(t)$ are the induced force vector due to the unit applied voltage to

the Lth actuator and the applied voltage to the Lth actuator. To model the test article in the finite element calculation, 20 by 40 four-node elements were used. Eq. (1) is transformed into the modal equation as follows:

$$[\underline{M}]\{\ddot{\eta}\} + [\underline{D}]\{\dot{\eta}\} + [\underline{K}]\{\eta\} = \sum_{L=1}^{M} \{\underline{F}_L\} V_L(t), \tag{2}$$

where

$$[\underline{M}] = [\Phi]^{\mathrm{T}}[M][\Phi] = [I], \quad [\underline{K}] = [\Phi]^{\mathrm{T}}[K][\Phi] = \mathrm{diag}(\omega_j^2),$$
$$[\underline{D}] = \mathrm{diag}(2\zeta_j\omega_j), \quad \{\underline{F}_L\} = [\Phi]^{\mathrm{T}}\{F_L\} \tag{3}$$

and $[\Phi]$, ω_j, and ζ_j are the mode matrix, the natural frequency, and the damping ratio, respectively. In Eq. (2), the damping matrix $[\underline{D}]$ is introduced for generality, and can be obtained from the modal testing. Actuation characteristics of PZT actuators in modal domain are specified by $\{\underline{F}_L\}$ and modal sensing characteristics can be obtained from the sensitivity of the laser displacement sensors and mode shape at the sensing points. Note that aerodynamic and other disturbance forces are not included at the present time.

3.2. Aerodynamic model

The linear relationship between the aerodynamic force acting on the nodal point and the vertical displacement of the nodal point is obtained from a DLM [22] as follows:

$$\{F\} = q[Q(k, M)]\{u\}, \tag{4}$$

where q, k, and M are the dynamic pressure, the reduced frequency, and the Mach number, respectively. By transforming nodal displacements into modal coordinates, generalized aerodynamic forces can be written as

$$\{\underline{F}\} = [\Phi]^{\mathrm{T}}\{F\} = q[\underline{Q}(k, M)]\{\eta\}, \tag{5}$$

where

$$[\underline{Q}(k, M)] = [\Phi]^{\mathrm{T}}[Q(k, M)][\Phi]. \tag{6}$$

The generalized aerodynamic influence coefficient $[\underline{Q}(k, M)]$ is a complex function of reduced frequency and flight condition. For a given Mach number and air density, $[\underline{Q}(k, M)]$ is calculated at several discrete reduced frequencies rather than as a continuous function of the circular frequency ω. Therefore, the aerodynamic influence coefficient matrices should be approximated as a rational function so that modern control theories are readily applicable to a resulting aeroelastic system. The minimum state method [23] approximates $[\underline{Q}(k, M)]$ by

$$[\tilde{\underline{Q}}(p)] = [A_0] + [A_1]p + [A_2]p^2 + [D](p[I] - [R])^{-1}[E]p, \tag{7}$$

where p is the nondimensionalized Laplace variable given as $p = sb/U_\infty$. Here b, s and U_∞ are the reference length, the Laplace variable and the free stream velocity, respectively. $[R]$ is a diagonal matrix whose diagonal terms are distinct aerodynamic poles. Physically weighted error function, in which each tabulated coefficient is weighted at each reduced frequency according to the

effect of an incremental error of this coefficient on aeroelastic characteristics of the system, is minimized during the optimization procedure. The details are referred to Ref. [23]. The overall approximation procedure mainly consists of two parts: a root finding problem and a determination of other unknown matrices. For a given root matrix $[R]$, the problem is to find the combination of $[A_0]$, $[A_1]$, $[A_2]$, $[D]$, and $[E]$ that best fits the tabular aerodynamic influence matrices at several discrete reduced frequencies. Proper selection of constraints makes this problem an iterative linear least-squares problem. On the other hand, aerodynamic poles are determined from an optimization algorithm for fixed matrices, $[A_0]$, $[A_1]$, $[A_2]$, $[D]$, and $[E]$. In this paper, a BFGS quasi-Newton method [26] is applied to optimize the root matrix $[R]$. By iteratively optimizing the root matrix and the other unknown matrices, we can approximate the aerodynamic force vector in continuous Laplace domain as follows:

$$\{\tilde{F}\} = q[\underline{\tilde{Q}}(V;s)]\{\eta\}. \tag{8}$$

3.3. Resulting aeroelastic model

Introducing the approximated aerodynamic force into Eq. (2) yields a state–space representation of the aeroelastic system.

$$\{\dot{x}\} = [A]\{x\} + [B]\{u\}, \quad \{y\} = [C]\{x\}, \tag{9}$$

where the state vector $\{x\}$ consists of the modal displacement $\{\eta\}$, the modal velocity $\{\dot{\eta}\}$, and the augmented aerodynamic states $\{x_a\}$; the control input $\{u\}$ is the applied voltages to the PZT actuators; $\{y\}$ is the measured displacement by the laser sensors. Note that the number of the aerodynamic states equals the number of aerodynamic poles. System matrix $[A]$ includes all aerodynamic effects such as apparent mass, aerodynamic damping and stiffness as well as structural mass, damping and stiffness. It should be noted that the system matrix $[A]$ is a function of air speed.

3.4. Model verification

First, the analysis results of the natural frequencies of the test article were compared with experimentally measured ones in Table 2, resulting in very good coincidence. Fig. 5 shows the first five mode shapes of the test article. Because of the swept back geometry, the combined behavior of the bending and torsion can be seen. However, you can see that the first mode is bending

Table 2
Natural frequencies of the test article in zero-flow condition

Mode number	Analysis (FEM)	Experiment
1	2.13	2.03
2	10.4	10.9
3	14.3	14.5
4	29.6	31.2
5	41.7	43.9

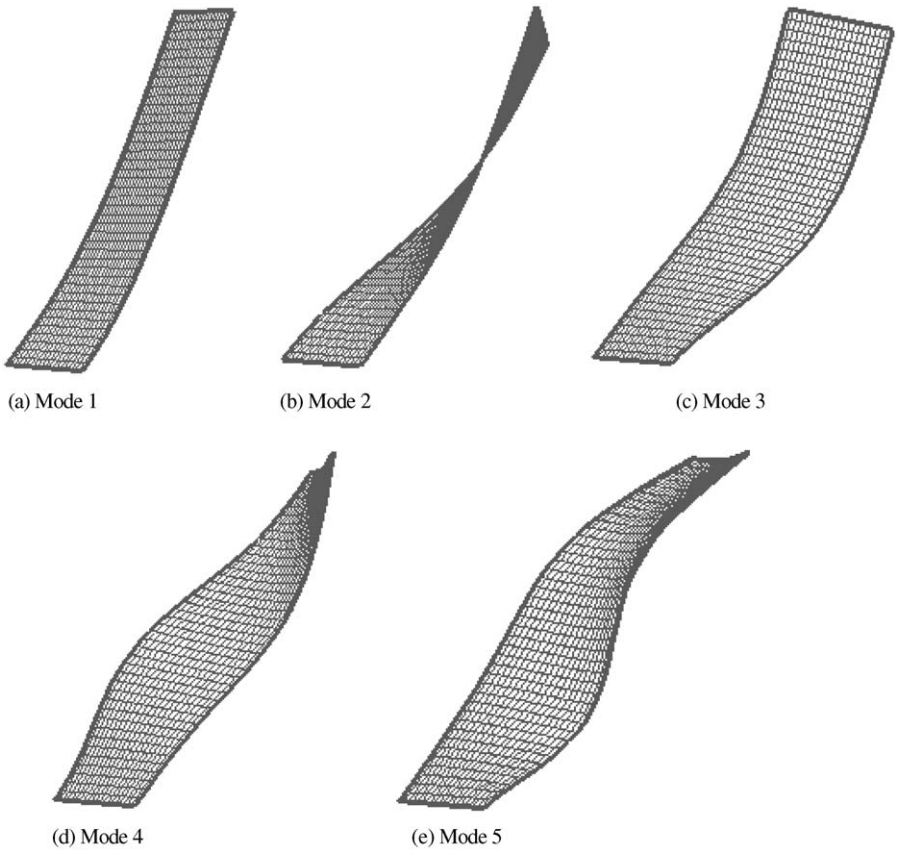

Fig. 5. Mode shapes of the lifting surface.

dominant, whereas the second mode is mainly torsion mode. The V–g method, one of the typical flutter analysis procedures, was applied to find the flutter speed of 15.1 m/s and the flutter frequency of 8.2 Hz. In the V–g method, the reference Mach number was taken to be 0.05, and the structural damping was not taken into account. Fig. 6 shows the V–f and V–g plots for the system, where you can see the coalescence of the first and second modes as the flow velocity increases. The V–g method gives us a good insight of the flutter phenomena, but it is difficult to consider the effects of control using V–g method.

A series of numerical models have been obtained by using the procedures described in Sections 3.1–3.3. It is found that 10 structural states (5 modes) and 3 aerodynamic states are sufficient to represent the plant dynamics over the flow range of interest. The stability of the system matrix $[A]$ is investigated to find the flutter speed of 16.6 m/s. The discrepancy is due to the inclusion of the structural damping and the truncation of some higher modes. The experimentally identified flutter speed is 17.1 m/s, and the flutter frequency is 7.2 Hz. Note that the flutter boundary is clear in the linear flutter analysis; however, it is not so obvious in the wind tunnel test. Therefore, the flow speed that caused very large dynamic amplitude was chosen as the experimental flutter speed

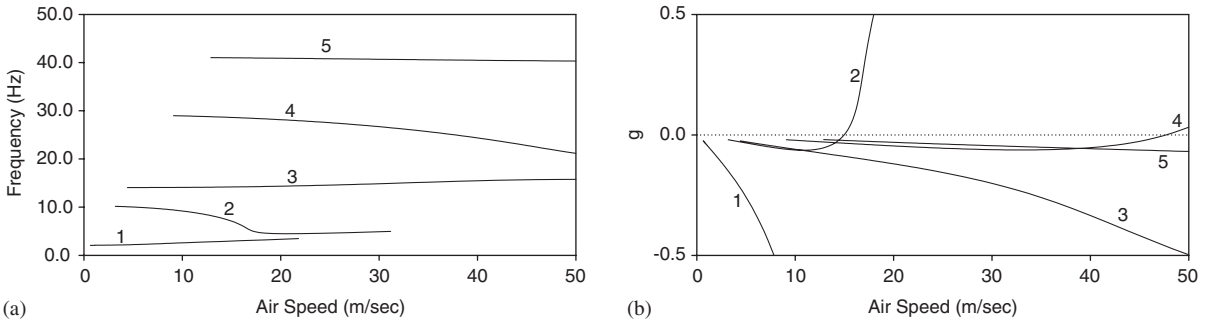

Fig. 6. V–f and V–g plots of the system.

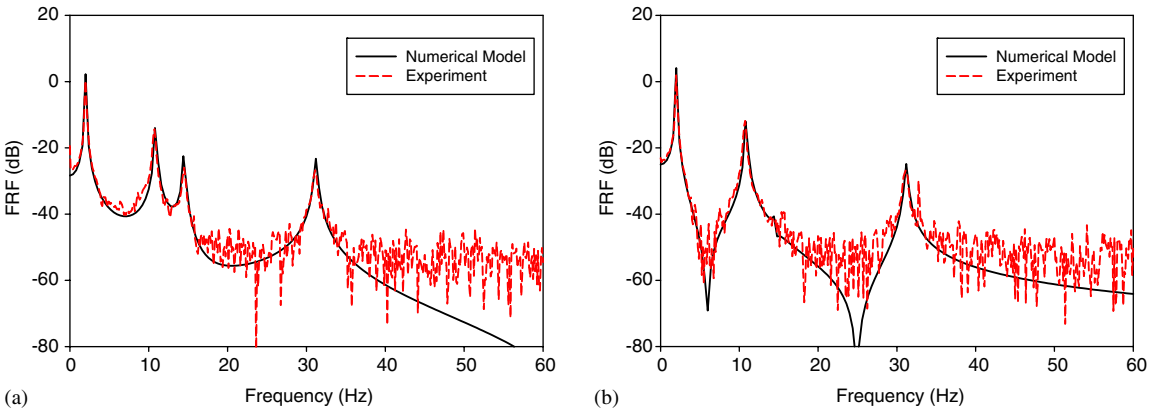

Fig. 7. Comparison of transfer functions: FRF between piezoactuators and (a) sensor 1 and (b) sensor 2.

throughout this study. This can be a reason why higher flutter speeds were obtained in the experiment compared with the analytical cases.

Finally, the numerical model of the actuation characteristics has been verified. The transfer functions between whole set of the piezoactuators and the laser sensors have been measured and compared with those of the numerical model in Fig. 7. Except for high-frequency roll-off region, the transfer function of the numerical model shows an excellent coincidence with experimentally obtained transfer function, which reveals that the established model properly describes not only natural vibration characteristics, but also the actuation properties.

4. Control design

4.1. Actuator pattern

The active control of flutter is viewed as a disturbance rejection problem for a linearly unstable or nearly unstable system as shown in Fig. 8. The locations of actuators as well as control

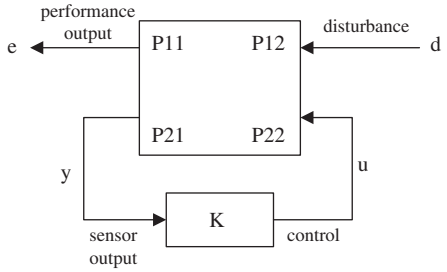

Fig. 8. A disturbance rejection problem.

algorithms affect significantly on the overall control performance. In this paper, 18 actuators are to be grouped into two equivalent actuator sets by common actuator commands. In the optimization, genetic algorithms were used as a searching method. Because the design variables are inherently in binary nature, genetic algorithms can be applied without any significant modification. The details are referred to Refs. [27,28].

The objective function for the actuator placement is based on the HSV analysis of P_{11} and P_{22}. Assuming the disturbance d as a white noise, we obtained the HSV $\bar{\gamma}_i$ and the corresponding principal direction $\bar{v}_i$ of the transfer function matrix P_{11}. The transfer function matrix P_{22} is dependent upon the actuator patterns. For each candidate patterns, the HSV γ_j and the corresponding principal direction v_j of the transfer function are calculated. The objective for the optimization was to maximize the objective function

$$J = \sum_i \sum_j \bar{\gamma}_i \gamma_j |\bar{v}_i^* v_j|, \tag{10}$$

where * denotes the complex conjugate operator. In Eq. (10), the objective function becomes larger when the actuators can excite the system modes as similarly as the external disturbances do. By proper genetic operations, the optimal pattern of the actuators is found as shown in Fig. 1, which seems to be effective especially for torsion mode actuation.

4.2. System augmentation

After obtaining the optimal actuator pattern, the controllers for the flutter suppression were designed using H_2- and μ-synthesized approaches. H_2 design follows the standard LQG design methods, and the weighting and covariance matrices were adjusted during the experiment. The detailed explanation for the design procedures for H_2 design is omitted here. The block interconnection of the whole system for the μ-synthesis design is shown in Fig. 9. The 2-input 2-output nominal plant model is obtained using Eq. (9) at the flow velocity of 16.5 m/s, which is quite close to the flutter boundary, and the system order is further reduced to 11 using balanced truncation in order to keep the controller order minimum. The open-loop nominal system P is augmented by the multiplicative uncertainty Δ_{del}, the weighting functions W_{del}, W_{dis}, W_{act}, W_{sen}, and W_{per}. In addition, parametric uncertainty Δ_{par} of the system is included to take into account the movement of the dominant pole. Since the damping value of the flutter mode varies

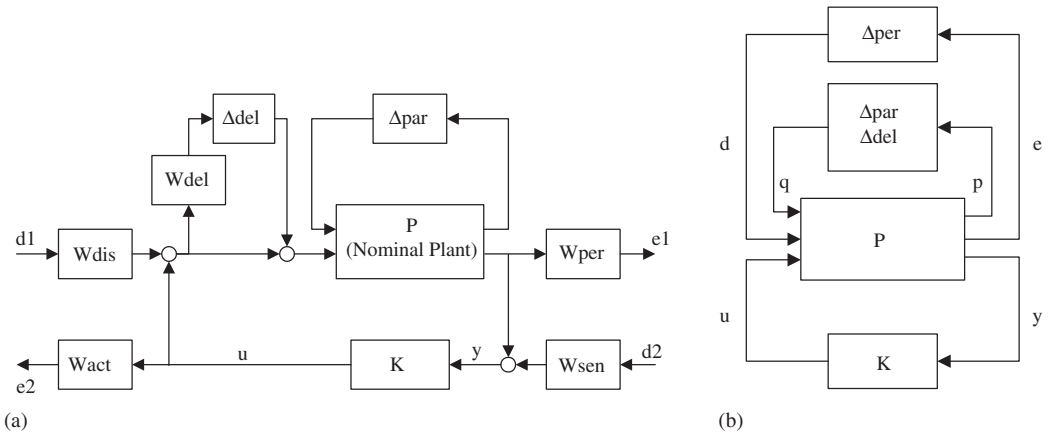

Fig. 9. Interconnection block diagram for the μ-synthesized controller design: (a) block diagram of the system and (b) augmented system closed with Δ_{per}.

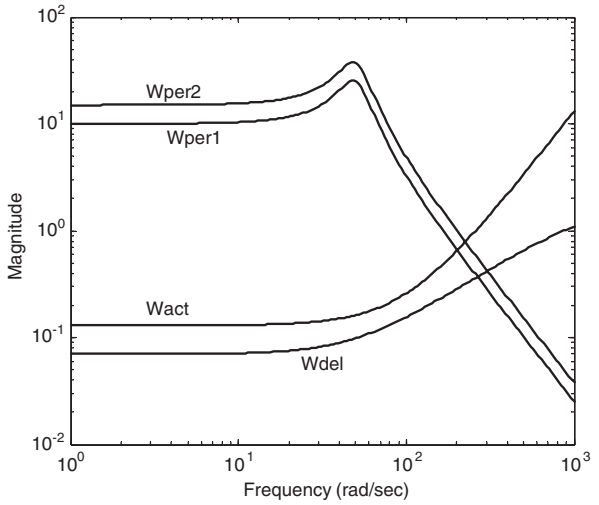

Fig. 10. Weight functions for μ-synthesis.

significantly without the frequency change near the flutter point, the system matrix is transformed into bi-diagonal form and only the damping term is treated as the parametric uncertainty [8]. The W_{dis} and W_{sen} are chosen to be constant as follows:

$$W_{\text{dis}} = \text{diag}(0.5, 0.5), \tag{11}$$

$$W_{\text{sen}} = \text{diag}(0.02, 0.02). \tag{12}$$

The constant weight for W_{sen} means that the sensor noise is assumed to be white noise, and the constant W_{dis} means that the disturbance exists over all the frequency range. The

magnitude plots of other weighting functions are presented in Fig. 10. The uncertainty error W_{del} indicates that the nonparametric modeling error could be up to 7% at low frequency and becomes larger in high-frequency region. W_{act} is used to limit control effort especially in high-frequency region. The chosen performance weighting function W_{per} means that good disturbance rejection (vibration suppression) is required only in low-frequency region, especially around flutter frequency. Unlike W_{del} and W_{act}, different scales are chosen for two channels of weighting functions W_{per} according to the expected relative sensor outputs at flutter condition.

4.3. μ-synthesis

Robust H_∞ performance is characterized by introducing a fictitious uncertainty block across disturbance/error channels and carrying out a robust stability analysis [29,30]. Therefore, the augmented system is cast to the form shown in Fig. 9(b) by introducing a fictitious uncertainty block Δ_{per}. By combining all the uncertainty blocks, Δ_{par}, Δ_{del}, and Δ_{per}, the following augmented uncertainty structure Δ is obtained:

$$\Delta = \begin{bmatrix} \Delta_{\mathrm{par}} & 0 & 0 \\ 0 & \Delta_{\mathrm{del}} & 0 \\ 0 & 0 & \Delta_{\mathrm{per}} \end{bmatrix}, \quad (\Delta_{\mathrm{par}} \in R, \Delta_{\mathrm{del}} \in C^{2\times 2}, \Delta_{\mathrm{per}} \in C^{4\times 4}). \tag{13}$$

It is well known that the robust performance is achieved if and only if

$$\max_{\omega} \mu_{\Delta}(F_L(P,K)(\mathrm{j}\omega)) < 1, \tag{14}$$

where F_L means the lower linear fractional transformation so that $F_L(P,K)$ is the transfer function from $\{q,d\}^{\mathrm{T}}$ to $\{p,e\}^{\mathrm{T}}$ in Fig. 9(b) when the augmented uncertainty block Δ is eliminated. For a complex system matrix M, $\mu_{\Delta}(M)$ is defined as follows:

$$\mu_{\Delta}(M) = \frac{1}{\min_{\Delta}\{\bar{\sigma}(\Delta) : \det(I - M\Delta) = 0\}}. \tag{15}$$

Therefore, the objective of μ-synthesis is to find the stabilizing controller K that minimizes the peak value of μ of the closed-loop transfer function $F_L(P,K)$

$$\min_{K} \max_{\omega} \mu_{\Delta}(F_L(P,K)(\mathrm{j}\omega)). \tag{16}$$

The optimization problem stated in Eq. (16) can be solved by an iterative approach, referred to as D–K iteration [30]. The obtained continuous controller is converted into discrete controller with the sampling frequency of 2 kHz, and implemented on a DSP board as described in Section 2.3.

5. Results and discussion

The designed H_2- and μ-synthesized controllers have been verified in the wind tunnel shown in Fig. 3. The test-section of the wind tunnel is open type so that sufficient disturbances in the flow

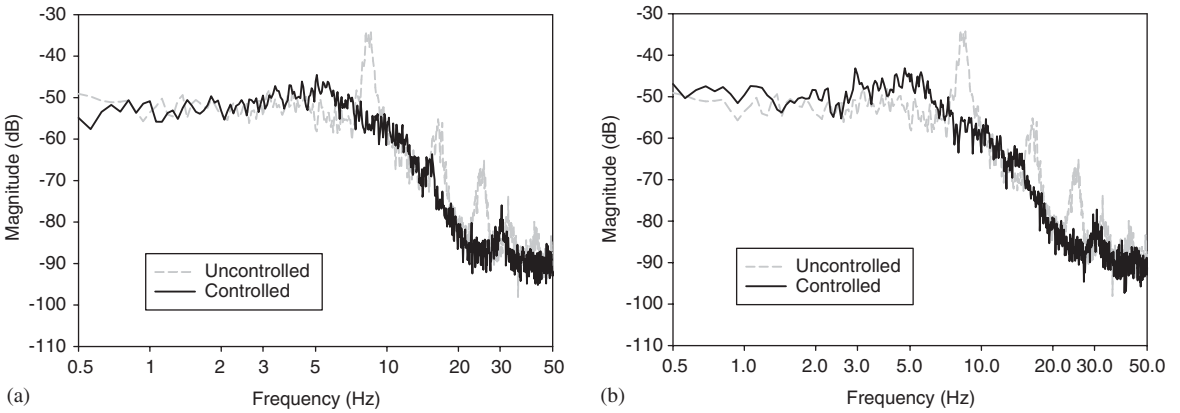

Fig. 11. Experimental flutter suppression results at the flow velocity of 17.0 m/s: (a) H_2 control and (b) μ-synthesized control.

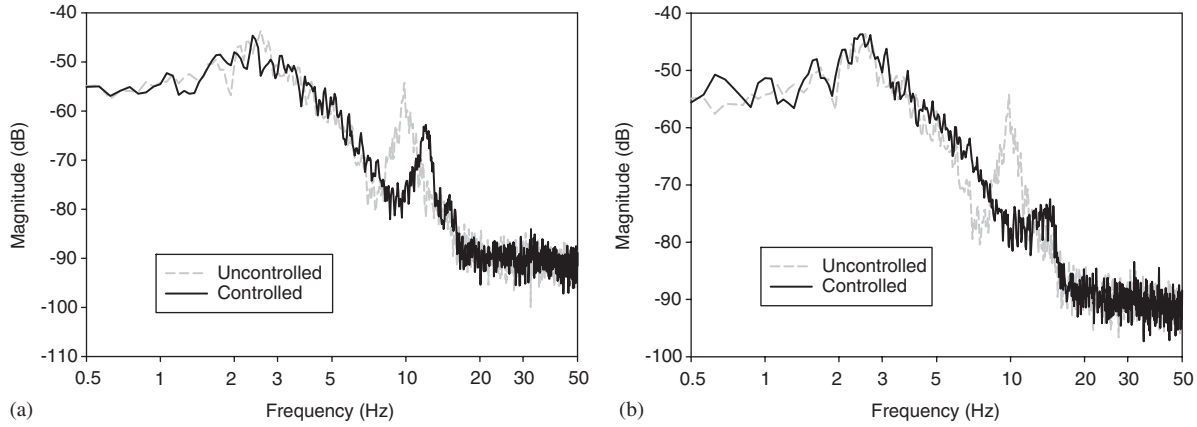

Fig. 12. Experimental flutter suppression results at the flow velocity of 10.0 m/s: (a) H_2 control and (b) μ-synthesized control.

excite the lifting surface. Figs. 11 and 12 show the representative active flutter control results, where the power spectra of the sensor 1 signals are presented for both uncontrolled and controlled cases. At the flow velocity of 17 m/s, which is slightly lower than the open-loop flutter speed, both controllers successfully suppress fluttering vibrations as shown in Fig. 11. Couples of large peaks in the open-loop responses can be seen at this speed, which are two- or three-times harmonics of the flutter mode due to structural nonlinearity with large amplitudes. Suppression of flutter mode made these harmonics disappear.

Two vibrational modes are dominant in the open-loop power spectra at the flow velocity of 10 m/s, which is quite below the flutter speed. It is clear from this observation that the vibration characteristics of the specimen are significantly affected by the airflow speed. Application of H_2

Table 3
Comparison of flutter speeds

Open/closed	Method	Flutter speed (m/s)	% Improvement[a]
Open loop	Analysis (V–g)	15.1	
	Analysis (Laplace)	16.6	
	Experiment	17.1	
Closed loop (experiment)	SISO LQG	18.2	6.4
	SISO μ-design	18.2	6.4
	MIMO LQG	18.8	9.9
	MIMO μ-design	19.0	11.1

[a]With respect to the experimental open-loop flutter speed.

controller is successful in eliminating the flutter mode, but induced another spurious mode of which frequency is a little higher than that of the open-loop second mode as shown in Fig. 12(a). It is observed that H_2 controller cannot be used under the flow velocity of 10 m/s because the spurious mode becomes unstable. In contrast, the μ-synthesized controller shows the improved behavior at this speed, and is stable even at 5 m/s.

In addition, experimental flutter speed can be increased up to 18.8 m/s using H_2 control, and up to 19.0 m/s using μ-synthesized control. Table 3 compares the flutter boundaries for various controls. When all the PZT actuators are connected to a single command and one laser sensor is used, the system becomes single-input single-output (SISO) system. In this case, the flutter speed can be increased up to 18.2 m/s (6.4% enhancement) for both controllers. The reason for the less performance is not due to controllers but due to the lack of the control force, especially in torsion direction.

6. Conclusions

This paper investigates active flutter suppression of a lifting surface using piezoelectric (PZT) actuation and modern control theory. A finite element method, a panel aerodynamic method, and the minimum state–space realization are utilized in the development of the equation of motion in state–space form. The resulting state–space representation is efficiently used for the analysis of the system and design of control laws with a modern control framework. PZT actuators, bonded symmetrically on the plate, are optimally grouped into two equivalent actuator sets using genetic algorithms to enhance controllability. H_2 and μ-synthesized control laws are designed and the flutter suppression performance is evaluated via the wind tunnel testing. In the μ synthesis design, a simple parametric uncertainty model is used to take into account the system changes with respect to varying airflow speed. The μ-synthesized controller shows improved behavior over a wide flow speed range. In order to further enhance the control performances, more effective torsional actuation mechanisms or actuators are requested.

References

[1] E.H. Dowell, E.F. Crawley, H.C. Curtiss Jr., D.A. Peters, R.H. Scanlan, F. Sisto, *A Modern Course in Aeroelasticity*, second ed., Kluwer Academic Publishers, Dordrecht, 1995.

[2] V. Mukhopadhyay, Flutter suppression control law design and testing for the active flexible wing, *Journal of Aircraft* 32 (1) (1995) 45–51.

[3] M.R. Waszak, S. Srinathkumar, Flutter suppression for the active flexible wing: a classical approach, *Journal of Aircraft* 32 (1) (1995) 61–67.

[4] W.M. Adams Jr., D.M. Christhilf, Design and multifunction tests of a frequency domain-based active flutter suppression system, *Journal of Aircraft* 32 (1) (1995) 52–60.

[5] A.G. Kelkar, S.M. Joshi, Passivity-based robust control with application to benchmark active control technology wing, *Journal of Guidance, Control, and Dynamics* 23 (5) (2000) 938–947.

[6] M.R. Waszak, Robust multivariable flutter suppression for benchmark active control technology wind-tunnel model, *Journal of Guidance, Control, and Dynamics* 24 (1) (2001) 147–153.

[7] J.S. Vipperman, R.L. Clark, M. Conner, E.H. Dowell, Experimental active control of a typical section using a trailing-edge flap, *Journal of Aircraft* 35 (2) (1998) 224–229.

[8] J.S. Vipperman, J.M. Barker, R.L. Clark, G.J. Balas, Comparison of μ- and H_2-synthesis controllers on experimental typical section, *Journal of Guidance, Control, and Dynamics* 22 (2) (1999) 278–285.

[9] J.J. Block, T.W. Strganac, Applied active control for a nonlinear aeroelastic structure, *Journal of Guidance, Control, and Dynamics* 21 (6) (1998) 838–845.

[10] I.D. Roy, W. Eversman, Adaptive flutter suppression of an unswept wing, *Journal of Aircraft* 33 (4) (1996) 775–783.

[11] Y. Zeng, S.N. Singh, Output feedback variable structure adaptive control of an aeroelastic system, *Journal of Guidance, Control, and Dynamics* 21 (6) (1998) 830–837.

[12] J.M. Barker, G.J. Balas, P.A. Blue, Gain-scheduled linear fractional control for active flutter suppression, *Journal of Guidance, Control, and Dynamics* 22 (4) (1999) 507–512.

[13] Z.-C. Yang, L.-C. Zhao, J.-S. Jiang, A semi-active flutter control scheme for a two-dimensional wing, *Journal of Sound and Vibration* 184 (1) (1995) 1–7.

[14] P.V.N. Gade, D.J. Inman, Active control of store-induced flutter in incompressible flow, *Journal of Aircraft* 35 (3) (1998) 454–461.

[15] R.G. Loewy, Recent developments in smart structures with aeronautical applications, *Smart Materials and Structures* 6 (1997) R11–R42.

[16] E.F. Crawley, J. de Luis, Use of piezoelectric actuators as elements of intelligent structures, *AIAA Journal* 25 (10) (1987) 1373–1385.

[17] K.B. Lazarus, E.F. Crawley, C.Y. Lin, Multivariable active lifting surface control using strain actuation: analytical and experimental results, *Journal of Aircraft* 34 (3) (1997) 313–321.

[18] J. Heeg, Analytical and experimental investigation on flutter suppression by piezoelectric actuation, NASA Technical Paper 3241, 1993.

[19] E.E. Forster, H.T.Y. Yang, Flutter control of wing boxes using piezoelectric actuators, *Journal of Aircraft* 35 (6) (1998) 949–957.

[20] J. D'Cruz, Active suppression of aircraft panel vibration with piezoceramic strain actuators, *Journal of Aircraft* 35 (1) (1998) 139–143.

[21] J.-H. Han, I. Lee, Analysis of composite plates with piezoelectric actuators for vibration control using layerwise displacement theory, *Composites Part B: Engineering* 29 (5) (1998) 621–632.

[22] E. Albano, W.P. Rodden, A doublet-lattice method for calculating lifting disturbances on oscillating surfaces in subsonic flows, *AIAA Journal* 7 (2) (1969) 279–285.

[23] M. Karpel, S.T. Hoadley, Physically weighted approximations of unsteady aerodynamic forces using the minimum-state method, NASA Technical Paper 3025, 1991.

[24] C. Nam, Y. Kim, T.A. Weisshaar, Optimal sizing and placement of piezo-actuators for active flutter suppression, *Smart Materials and Structures* 5 (2) (1996) 216–224.

[25] K.B. Lim, R.C. Lake, J. Heeg, Effective selection of piezoceramic actuators for an experimental flexible wing, *Journal of Guidance, Control, and Dynamics* 21 (5) (1998) 704–709.

[26] A.D. Belegundu, T.R. Chandrupatla, *Optimization Concepts and Applications in Engineering*, Prentice-Hall, Englewood Cliffs, NJ, 1999.
[27] J.-H. Han, I. Lee, Active damping enhancement of composite plates with electrode designed piezoelectric materials, *Journal of Intelligent Material Systems and Structures* 8 (3) (1997) 249–259.
[28] J.-H. Han, I. Lee, Optimal placement of piezoelectric sensors and actuators for vibration control of a composite plate using genetic algorithms, *Smart Materials and Structures* 8 (2) (1999) 257–267.
[29] J.C. Doyle, K. Glover, P.P. Khargonekar, B.A. Francis, State–space solutions to standard H_2/H_∞ control problems, *IEEE Transactions on Automatic Control* 34 (1989) 831–847.
[30] G.J. Balas, J.C. Doyle, K. Glover, A. Packard, R. Smith, *User's Guide*, *μ-Analysis and Synthesis Toolbox*, Version 3, The Mathworks Nattick, MA, 1998.